ACS OMEGA

Open Access

http://pubs.acs.org/journal/acsodf

Article

Enhanced Method for the Synthesis and Comprehensive Characterization of 1-(4-Phenylquinolin-2-yl)propan-1-one

Satheeshkumar Rajendran,* Rodrigo Montecinos, Jonathan Cisterna, Kolandaivel Prabha, Karnam Jayarampillai Rajendra Prasad, Sushesh Srivatsa Palakurthi, Alaa A. A Aljabali, Gowhar A. Naikoo, Vijay Mishra, Roberto Acevedo, Koray Sayin, Nitin Bharat Charbe,* and Murtaza M. Tambuwala*

Cite This: *ACS Omega* 2023, 8, 43573−43585

Read Online

ACCESS | Metrics & More | Article Recommendations | Supporting Information

ABSTRACT: We present an enhanced method for synthesizing a novel compound, 1-(4-phenylquinolin-2-yl)propan-1-one (**3**), through the solvent-free Friedländer quinoline synthesis using poly(phosphoric acid) as an assisting agent. The crystal structure of compound **3** is analyzed using FT-IR, and the chemical shifts of its ^{1}H- and ^{13}C NMR spectra are measured and calculated using B3LYP/6-311G(d,p), CAM-B3LYP/6-311G(d,p), and M06-2X/6-311G(d,p) basis sets in the gas phase. Additionally, the optimized geometry of quinoline **3** is compared with experimental X-ray diffraction values. Through density functional theory calculations, we explore various aspects of the compound's properties, including noncovalent interactions, Hirshfeld surface analysis, nonlinear optical properties, thermodynamic properties, molecular electrostatic potential, and frontier molecular orbitals. These investigations reveal chemically active sites within this quinoline derivative that contribute to its chemical reactivity.

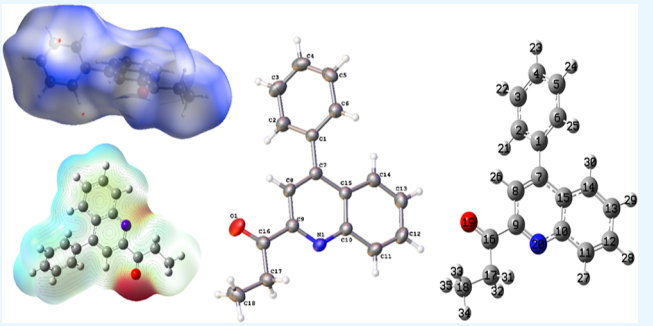

1. INTRODUCTION

The quinoline scaffold is an abundant heterocyclic structural core that exists in numerous naturally found quinoline alkaloids.[1] The quinoline skeleton is used as a template for several synthetic compounds with various pharmacological properties, including antimalarial, anti-inflammatory, antiasthmatic, antibacterial, antiviral, and antihypertensive and tyrosine kinase inhibiting agents.[1−8] Researchers continue to seek new methodologies and products for synthesizing quinoline-based moieties. Various classic techniques to synthesize quinoline moiety include the Skraup,[9,10] Doebner−von Miller,[11] Pfitzinger,[12] Conrad−Limpach,[13] Combes syntheses,[14] and Povarov reactions.[15,16] Among them, a notable approach for attaining quinolines and related polyheterocycles involves Friedländer quinoline synthesis.[17−19] Among these methods, the Friedländer synthesis is the most effective and prominent protocol for the synthesis of quinolines in recent years.[19−23] It has become the evergreen synthetic approach to prepare quinoline derivatives by the condensation of easily accessible 2-aminoarylketones with carbonyl compounds possessing a reactive methylene group, followed by cyclodehydration.[24−28] The most exciting method for improving organic synthesis is continuously reporting new methodologies and catalytic reactions. A solvent-free synthesis is an essential synthetic approach from the perspective of synthetic organic chemistry. Recently, sulfuric acid functionalized heterogeneous catalysts have developed as user-friendly catalysts due to their remarkable advantages over homogeneous catalytic systems, such as prolonged reaction times, enhanced selectivity, the comfort of product purification, ease of operation, low turnover frequency, and surplus amount of catalyst.[29−31]

Based on the above insight, quinoline derivatives were developed by condensing 2-aminoarylketones with carbonyl compounds owning a reactive methylene group, followed by cyclodehydration. Quantum chemical calculations were conducted at the B3LYP/6-311G(d,p), CAM-B3LYP/6-311G(d,p), and M06-2X/6-311G(d,p) levels of theory in the gas phase to optimize the structure, determine vibrational frequencies, chemical shift values using NMR analysis, Hirshfeld surface analysis, highest occupied molecular orbital (HOMO)/lowest unoccupied molecular orbital (LUMO), molecular electrostatic potential (MEP) maps, nonlinear optical (NLO) properties, and thermodynamic proper-

Received: June 19, 2023
Revised: October 16, 2023
Accepted: October 20, 2023
Published: November 8, 2023

ties.[32−37] Here, we would like to report a convenient and straightforward workup method for the synthesis of quinoline molecule (**3**) using freshly prepared polyphosphoric acid (PPA)[38−41] (P_2O_5 in H_3PO_4) under solvent-free conditions from 2-aminobenzophenone (**1**) and pentan-2,3-dione (**2**) through Friedländer quinoline synthesis.

2. INSTRUMENTATION METHODS

2.1. FT-IR and NMR Analysis. Fourier transform infrared (FT-IR) BRUKER brand (VECTOR 22) was used to record the FT-IR with spectral data collected in the range 4000−400 cm^{-1}. FT-Raman spectrum was recorded using a WiTec Alpha 300 RA Raman-AFM. BRUKER AVANCE III HD-400 [400 MHz (^1H) and 100 MHz (^{13}C)] spectrometers used tetramethyl silane (TMS) as an internal reference for ^1H NMR and ^{13}C NMR. The chemical shifts are observed in parts per million (ppm). Coupling constants (J) are reported in hertz (Hz). The terms J_o and J_m refer to the ortho coupling constant and meta coupling constant. The terms s, d, t, and dd refer to singlet, doublet, triplet, and doublet of doublet, respectively, and bs refers to a broad singlet. A liquid chromatography−mass spectrometry (LC−MS) experiment was conducted using a UHPLC Eksigent1 coupled with ABSciex1MS detector Triple Quad 4500 model equipment. The sample was injected using a syringe, and the data were acquired in a range of 100.0−600.0 Da, at 200 Da s^{-1} under positive polarity.

2.2. Single-Crystal XRD Analysis. The 1-(4-phenylquinolin-2-yl)propan-1-one (**3**) crystals were chosen for measurement. The diffraction data were collected at 296 K on a Bruker D8 Venture diffractometer equipped with a bidimensional CMOS Photon 100 detector. The monochromatic Mo Kα (λ = 0.71073 Å) radiation with a graphite monochromator was used for the data collection. The acquired diffraction frames were integrated using the APEX3 package,[42] and it was corrected for absorptions with SADABS.[43] The structure of 1-(4-phenylquinolin-2-yl)-propan-1-one (**3**) was solved by intrinsic phasing[44] using the OLEX2 program.[45] Then, the obtained structure was refined with full-matrix least-squares methods based on F^2 (SHELXL-2014).[44] The non-hydrogen atoms were refined with anisotropic displacement parameters during the refinement process of the crystal structure. All hydrogen atoms were included in their calculated positions, assigned fixed isotropic thermal parameters, and confined to riding their parent atoms.

2.3. DFT Computational Studies. Molecular structure of the compound in the ground state was optimized, from crystal structure as starting point, using three density functional theory (DFT) methods: B3LYP[46] the long-range corrected version of B3LYP: CAM-B3LYP[47] and the Minnesota 06 functional as M06-2X.[48] All DFT calculations, such as geometrical parameters, energy, IR and NMR spectra, atomic charges, HOMO and LUMO energy, and dipole moment, etc., were performed with the 6-311G(d,p)[49] basis set level. GaussView 5.0.9[50] and Gaussian 09AS64L-G09RevD.01[51] package programs were used to do numerical calculations. ChemBioDraw Ultra Version (13.0.0.3015)[52] was used as utility program. Energy gap (E_{gap}) global hardness (η), global softness (S), global electronegativity (χ), and chemical potential (μ) were calculated to determine the reactivity of studied compound (**3**) with eqs 1−5,[53−55] respectively

$$E_{gap} = E_{LUMO} - E_{HOMO} \quad (1)$$

$$\eta = \frac{E_{LUMO} - E_{HOMO}}{2} \quad (2)$$

$$S = \frac{1}{2\eta} \quad (3)$$

$$\chi = \frac{-(E_{HOMO} + E_{LUMO})}{2} \quad (4)$$

$$\mu = -\chi \quad (5)$$

2.4. Hirshfeld Surface Analyses. Hirshfeld surface analysis[56] was performed using CrystalExplorer 17.5.[57] This analysis consists of d_{norm} surface plots and 2D (two-dimensional) fingerprint plots.[58] The mapped electrostatic potentials on the Hirshfeld surfaces using the BLYP/6-31G(d,p) level of theory over a range of ±0.002 au using the TONTO computational package integrated into the program CrystalExplorer.[59] The analysis was conducted using the crystallographic information file (CIF) of 1-(4-phenylquinolin-2-yl)propan-1-one (**3**) as the input. The normalized contact distance (d_{norm}) was described in terms of d_e, d_i, and vdW radii of the atoms was calculated using eq 6, where d_e and d_i are the lengths from the Hirshfeld isosurface to the nearest external and internal nucleus, respectively, and vdW corresponds to the van der Waals radii of atoms.[60,61]

$$d_{norm} = \frac{d_i + r_i^{vdw}}{r_i^{vdw}} + \frac{d_e + r_e^{vdw}}{r_e^{vdw}} \quad (6)$$

3. EXPERIMENTAL DETAILS

3.1. General. All reagents and chemicals used in the study were purchased from AKSci and Sigma-Aldrich. Unless otherwise indicated, other reagents were obtained from commercial suppliers. Relevant references were given when known compounds were prepared according to the literature procedures. The purity of the synthesized product was demonstrated by TLC silica gel 60 F254 25 aluminum foil 20 × 20 C (purchased from Merck) using petroleum ether and ethyl acetate in the ratio of 95:5 as preparing solvents. Melting points (Mp) were shown on a Kofler Thermogerate apparatus and were uncorrected. They are displayed in degrees of centigrade (°C).

3.2. Synthesis. *3.2.1. General Procedure for Preparation of 1-(4-Phenylquinolin-2-yl)propan-1-one (**3**).* A mixture of the 2-aminobenzophenone (**1**, 1 mmol) and pentan-2,3-dione (**2**, 1.2 mmol) was heated for 1 h in the presence of freshly prepared PPA reagent (P_2O_5 in H_3PO_4) as a catalyst without any solvent at 90 °C. The completion of the reaction was analyzed by TLC. The reaction was quenched with an excess amount of saturated sodium carbonate solution (30 mL). Then, the obtained solid was filtered, washed with water, extracted with CH_2Cl_2 (3 × 10 mL), and dried over anhydrous sodium sulfate. Evaporation of the solvent was followed by purification via recrystallization from CH_2Cl_2 to yield the pure product 2-acetyl-4-arylquinoline (**3**).

White solid; yield 82%, mp 111−112 °C. FT-IR (KBr, cm^{-1}) (Figure S1) ν_{max}: 3055, 2947, 1697, 1558, 1435, 1373, 1172, 1010.

^1H NMR (400 MHz, $CDCl_3$) (Figure S5) (ppm): δ 1.30 (t, 3H, CH_3, J = 7.20 Hz), 3.46 (q, 2H, CH_2, J = 7.20 Hz), 7.47−7.56 (m, 5H, C_2-, C_3-, C_4-, C_5-, C_6-H), 7.59 (t, 1H, C_{12}-H, J = 8.00 Hz), 7.78 (t, 1H, C_{13}-H, J = 8.00 Hz), 7.97 (d, 1H, C_{14}-

https://doi.org/10.1021/acsomega.3c04360
ACS Omega 2023, 8, 43573−43585

Scheme 1. Synthesis of 1-(4-Phenylquinolin-2-yl)propan-1-one (3)

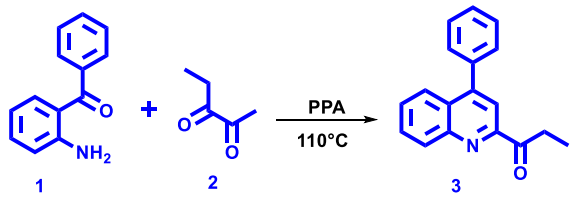

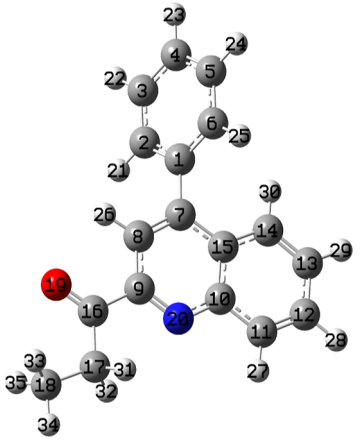

Figure 1. Optimized structure of molecule **3** at the B3LYP/6-311G(d,p) level in vacuum.

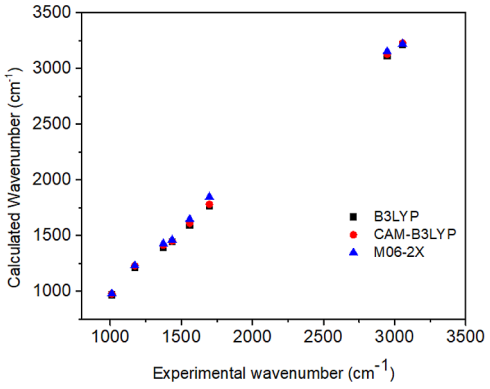

Figure 2. Distribution graphs between experimental and calculated stretching frequencies for molecule **3**.

H, J = 8.00 Hz), 8.08 (s, 1H, C_8-H), 8.26 (d, 1H, C_{11}-H, J = 8.00 Hz).

^{1}H NMR (400 MHz, DMSO-d_6) (Figure S6) (ppm): δ 1.18 (t, 3H, CH_3, J = 7.20 Hz), 3.41 (q, 2H, CH_2, J = 7.20 Hz), 7.56−7.64 (m, 5H, C_2-, C_3-, C_4-, C_5-, C_6-H), 7.75 (t, 1H, C_{12}-H, J = 8.00 Hz), 7.89−7.95 (m, 3H, C_8-, C_{13}, C_{14}-H), 8.26 (d, 1H, C_{11}-H, J = 8.00 Hz).

^{13}C NMR (100 MHz, $CDCl_3$) (Figure S10) (ppm): δ 8.14, 30.91, 118.36, 125.85, 128.09, 128.44, 128.58, 128.63, 129.58, 129.73, 130.93, 137.83, 147.83, 149.39, 152.61, 203.29.

^{13}C NMR (100 MHz, DMSO-d_6) (Figure S11) (ppm): δ 8.42, 30.72, 118.09, 125.93, 127.73, 129.34, 129.65, 129.84, 130.92, 130.98, 137.52, 147.59, 149.40, 152.64, 202.51. LC−MS for ($C_{18}H_{15}NO$) m/z (%): 261.9 (M + 1, 100).

Table 2. ^{1}H-NMR Chemical Shift δ (ppm) (Figures S5−S9)

atoms	$CDCl_3$	DMSO-d_6	B3LYP/6-311G(d,p)
C2(H)	7.47−7.56	7.56−7.64	7.56
C3(H)			7.51
C4(H)			7.52
C5(H)			7.64
C6(H)			7.66
C8(H)	8.08	7.89−7.95	8.3
C11(H)	8.26	8.26	8.38
C12(H)	7.59	7.75	7.79
C13(H)	7.78	7.89−7.95	7.6
C14(H)	7.97	7.89−7.95	8.14
C17(H2)	3.46	3.41	3.41
C18(H3)	1.30	1.18	1.19

Table 3. ^{13}C-NMR Chemical Shift δ (ppm) (Figures S10−S14)

atoms	$CDCl_3$	DMSO-d_6	B3LYP/6-311G(d,p)
C1	137.83	137.52	160.92
C2	129.58	129.34	150.82
C3	128.44	129.65	147.11
C4	128.58	129.65	148.21
C5	128.58	129.65	149.43
C6	129.58	129.34	149.69
C7	149.39	149.40	171.32
C8	118.36	118.09	137.32
C9	152.61	152.64	171.25
C10	147.83	147.59	167.82
C11	130.93	130.92	152.63
C12	129.73	130.98	148.56
C13	128.63	129.84	147.72
C14	128.09	127.73	145.88
C15	125.85	125.93	147.44
C16	203.29	202.51	220.35
C17	30.91	30.72	50.15
C18	8.14	8.42	24.14

Table 1. FT-IR Frequencies (cm^{-1}) (Figures S1−S4)

assignments	experimental	B3LYP	CAM-B3LYP	M06-2X
$\nu_{CH\ asymmetric}$	3055.24	3209.2−3163.7	3227.9−3182.1	3219.3−3170.3
$\nu_{CH\ symmetric}$	2947.23	3108.9−3104.4	3128.0−3123.2	3150.8−3139.7
−C=O	1697.36	1764.6	1779.9	1844.9
−C=N	1558.48	1592.2	1610.7	1646.0
=C−H	1435.04	1443.1	1450.2	1458.7
H−C−H	1373.20	1392.9	1412.3	1427.2
N−C−C=O	1172.72	1215.3	1228.6	1230.4
Ph ring	1010.70	967.5	975.4	978
R^2		0.9849	0.9838	0.9715

https://doi.org/10.1021/acsomega.3c04360
ACS Omega 2023, 8, 43573−43585

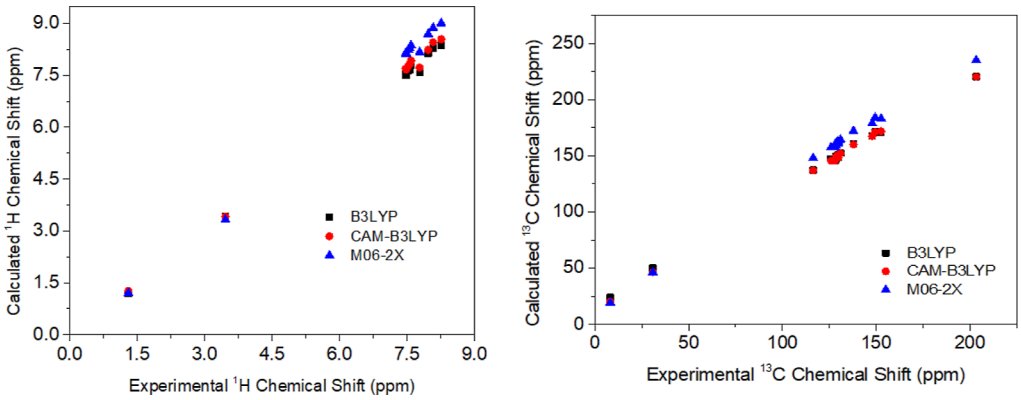

Figure 3. Distribution graphs between calculated and experimental ^{1}H and ^{13}C NMR chemical shifts for molecule **3**.

4. RESULTS AND DISCUSSION

4.1. Synthesis. The 2-aminobenzophenone (**1**) was treated with pentan-2,3-dione (**2**) in the presence of freshly prepared PPA as a catalyst without any solvent at 90 °C for 1 h to yield 82% of 1-(4-phenylquinolin-2-yl)propan-1-one (**3**) (Scheme 1).

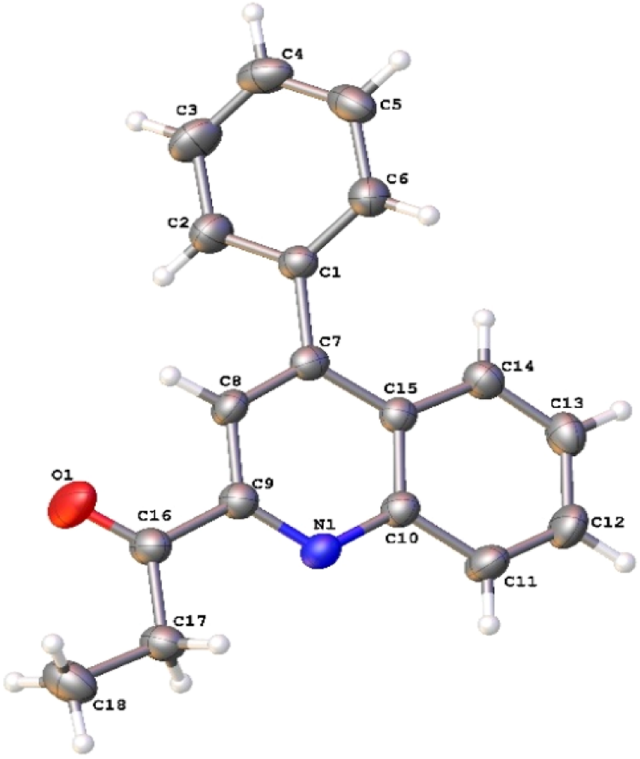

Figure 4. ORTEP plot for molecule **3**. Thermal ellipsoids were drawn with 50% of probability.

Table 4. Crystal Data Parameters for Molecule 3

empirical formula	$C_{18}H_{15}NO$
CCDC number	2077085
formula mass, g mol^{-1}	261.31
collection T, K	296.86
crystal system	Orthorhombic
space group	$P2_12_12_1$
a (Å)	7.2696(6)
b (Å)	10.6810(8)
c (Å)	17.8044(14)
V (Å^3)	1382.45(19)
Z	4
ρ_{calcd} (g cm^{-3})	1.255
crystal size (mm)	0.25 × 0.23 × 0.19
F(000)	552.0
abs coeff (mm^{-1})	0.078
2θ range (deg)	5.958 to 56.534
range h, k, l	−9/9, −14/14, −23/23
no. total refl.	26,163
no. unique refl.	3433 [Rint = 0.0836, Rsigma = 0.0468]
comp. θ_{max} (%)	99.9
max/min transmission	0.983/0.980
data/restraints/parameters	3433/0/183
final R [$I > 2\sigma(I)$]	$R1$ = 0.0526, wR2 = 0.0980
R indices (all data)	$R1$ = 0.0976, wR2 = 0.1162
goodness of fit/F^2	1.022
largest diff. peak/hole (eÅ^{-3})	0.23/−0.15
Flack parameter	−0.7(10)

4.2. Computational Methods. *4.2.1. Full Optimizations.* The studied compound is fully optimized at each computational level and the optimized structure of molecule **3** is obtained at B3LYP/6-311G(d,p) in the gas phase are given in Figure 1.

4.2.2. FT-IR Analysis. FT-IR spectrum of molecule **3** is calculated at B3LYP/6-311G(d,p), CAM-B3LYP/6-311G-(d,p), and M06-2X/6-311G(d,p) levels of theory, and experimental stretching frequency values are represented as a distribution graph in Figure 2. Furthermore, correlation coefficient for each level. The calculated and experimental stretching frequencies are harmonic frequencies. Some stretching frequencies and correlation coefficients (R^2) are shown in Table 1.

The B3LYP/6-311G(d,p) level is the best calculation level in Table 1 and Figure 2 due to the fact that the highest R^2 is obtained in this level. After those computational results in the B3LYP/6-311G(d,p) level are given for other computational parts. In the FT-IR (KBr, cm^{-1}) spectrum (Figure S1) of molecule **3**, the C═O stretching at 1697 cm^{-1} and C═N stretching at 1558 cm^{-1} were found. The theoretical values of FT-IR, which are given by B3LYP/6-311G(d,p) (Figure S2), CAM-B3LYP/6-311G(d,p) (Figure S3), and M06-2X/6-311G(d,p) (Figure S4) levels of theory are mostly in good agreement, as shown in Table 1.

4.2.3. FT-NMR Analysis. The ^{1}H NMR (400 MHz) and ^{13}C NMR (100 MHz) spectra of molecule **3** were recorded in

https://doi.org/10.1021/acsomega.3c04360
ACS Omega 2023, 8, 43573−43585

Table 5. Optimized Geometrical Parameters (Bond Lengths, Bond Angles, and Dihedral Angels) of Molecule 3 Using B3LYP/6-311G(d,p), CAM-B3LYP/6-311G(d,p), and M06-2X/6-311G(d,p) Levels of Theory in Comparison with Experimental XRD Studies

parameters	bond length (A)		parameters	bond angles (deg)		parameters	dihedral (deg)	
	XRD	B3LYP/6-311G(d,p)		XRD	B3LYP/6-311G(d,p)		XRD	B3LYP/6-311G(d,p)
C1−C2	1.39	1.39	C1−C2−C3	120.8	120.61	C2−C1−C7−C8	−47.23	−55.86
C2−C3	1.39	1.39	C2−C3−C4	120.29	120.15	C6−C1−C7−C15	132.91	121.9
C3−C4	1.37	1.39	C3−C4−C5	119.73	119.69	C7−C15−C14−C13	−178.86	−179.78
C4−C5	1.37	1.39	C4−C5−C6	120.59	120.2	C7−C8−C9−N1	−0.97	0.1
C5−C6	1.38	1.39	C5−C6−C1	120.08	120.54	C9−N1−C10−C11	−177.84	−178.85
C1−C7	1.49	1.49	C6−C1−C7	122.14	121.08	C9−N1−C10−C15	1.29	0.587
C7−C8	1.37	1.37	C1−C7−C8	118.58	118.82	C9−C16−C17−C18	179.8	179.85
C7−C15	1.42	1.43	C1−C7−C15	123.56	122.34	N1−C9−C16−C17	4.27	0.369
C8−C9	1.41	1.41	C7−C8−C9	120.52	119.9	N1−C10−C11−C12	178.71	178.52
C9−N1	1.32	1.31	C7−C15−C14	124.25	123.88			
N1−C10	1.37	1.36	C8−C9−N1	123.52	123.76			
C10−C11	1.41	1.42	C8−C9−C16	118.7	118.55			
C10−C15	1.43	1.42	C9−N1−C10	117.4	118.01			
C11−C12	1.36	1.36	N1−C10−C11	117.73	117.74			
C12−C13	1.4	1.41	N1−C10−C15	123.03	122.73			
C13−C14	1.36	1.37	C10−C11−C12	120.52	120.58			
C14−C15	1.42	1.42	C10−C15−C14	118.12	118.37			
C9−C16	1.51	1.51	C11−C12−C13	120.48	120.08			
C16−O1	1.21	1.21	C12−C13−C14	120.61	120.66			
C16−C17	1.49	1.51	C13−C14−C15	121.03	120.756			
C17−C18	1.51	1.52	C9−C16−C17	118.37	117.73			
			C9−C16−O1	119.4	119.67			
			C16−C17−C18	113.8	112.87			

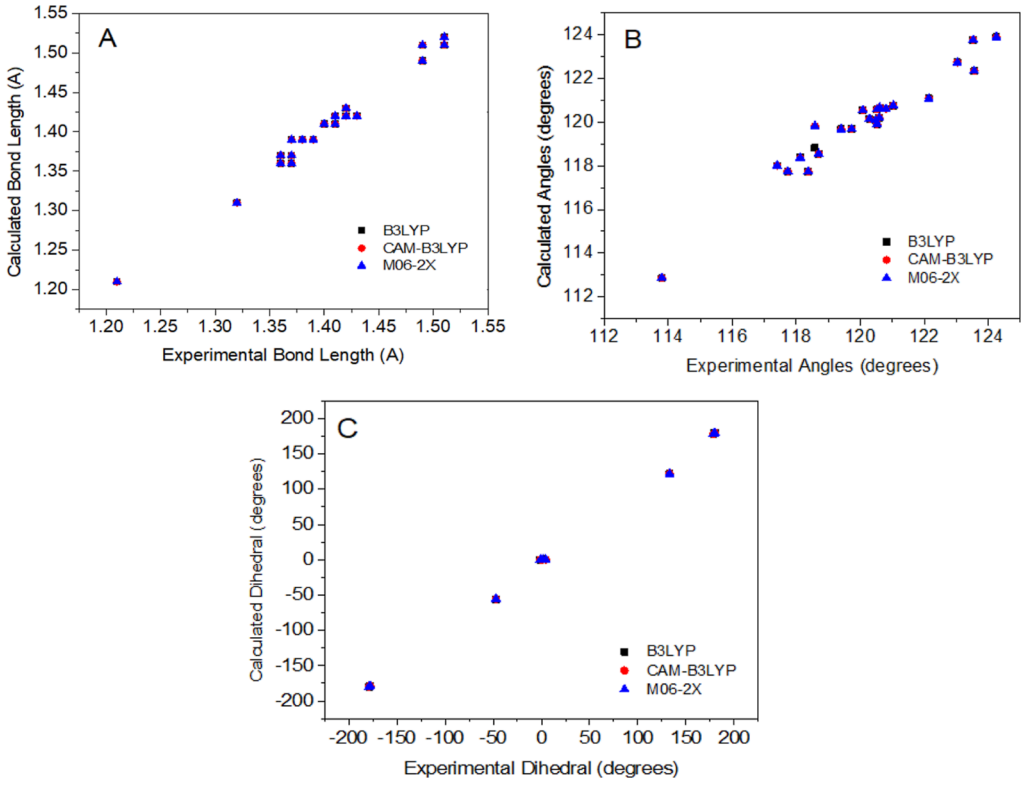

Figure 5. Correlation of experimental and calculated structural parameters for molecule **3**. (A) Bond length, (B) bond angles, and (C) dihedral angles.

CDC_{l3} and DMSO-d_6 with TMS as the internal standard. Simulated ^{1}H and ^{13}C NMR spectra were calculated for each level. Experimental and calculated results in the B3LYP/6-311G(d,p) level for molecule **3** are given in Tables 2 and 3. For other computational results, they are given in Tables S1 and S2. Within ^{1}H NMR by using $CDCl_3$ (Figure S5) or

https://doi.org/10.1021/acsomega.3c04360
ACS Omega 2023, 8, 43573−43585

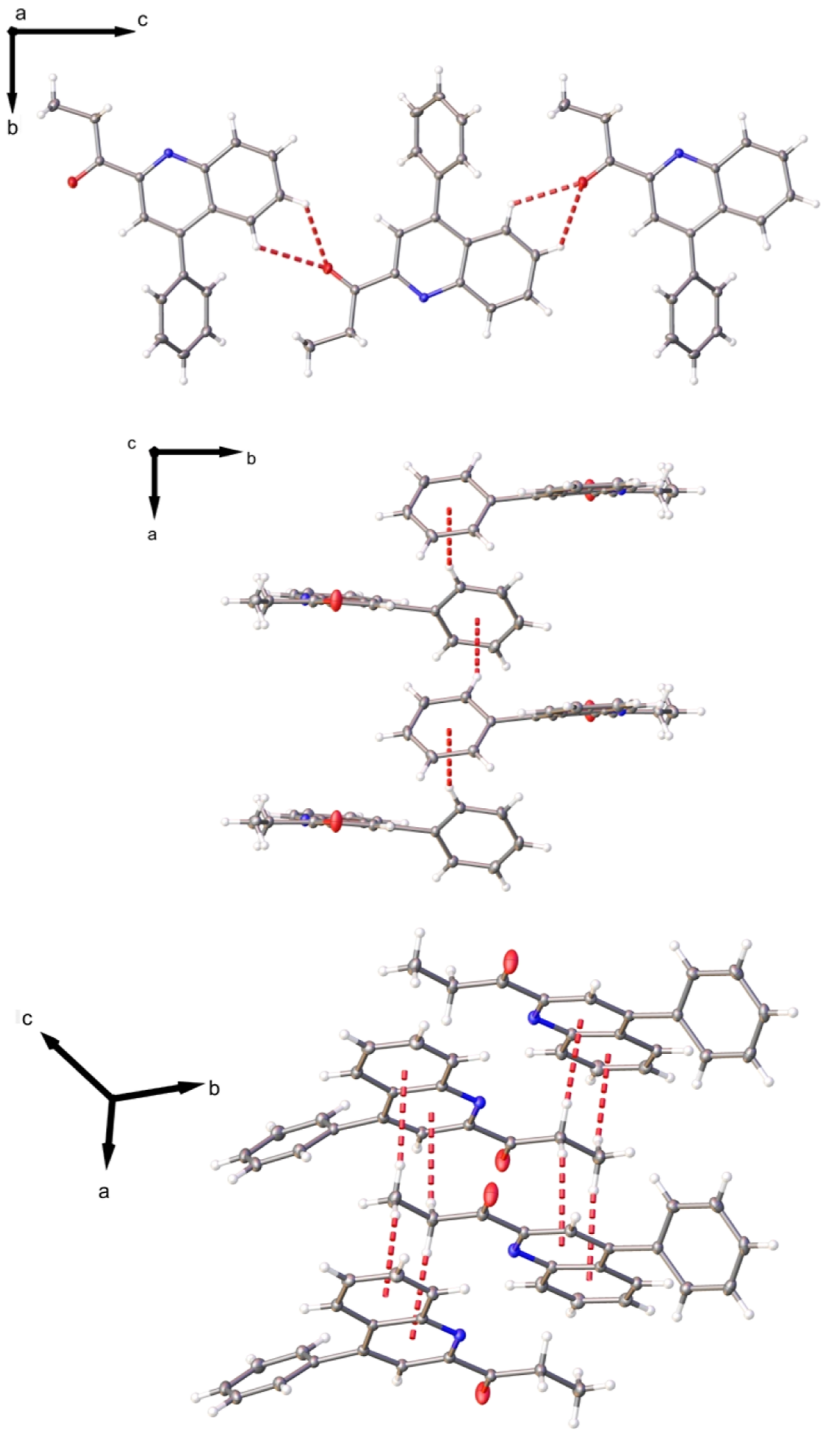

Figure 6. Crystal packing of molecule **3**.

Table 6. Hydrogen Bond Interactions for Molecule 3

atoms	D−H	H···A	D···A	D−H···A
C13−H13···O1[b]	0.93	2.732	3.314(4)	121.5
C14−H14···O1[b]	0.93	2.829	3.366(4)	117.8
C2−H2···CNT1[c,a]	0.93	2.739	3.611(3)	159.4
C17−H17B···CNT2[d,a]	0.97	2.841	3.639(4)	146.7
C18−H18C···CNT3[d,a]	0.93	2.739	3.611(3)	159.4

[a]CNT = centroid; 1: C1/C2/C3/C4/C5/C6; 2: C7/C8/C9/N1/C10/C15; 3: C10/C11/C12/C13/C14/C15. [b]3/2 − *x*, 1 − *y*, −1/2 − *z*. [c]−1/2 + *x*, 1/2 − *y*, 1 − *z*. [d]−1/2 + *x*, 3/2 − *y*, 1 − *z*.

DMSO-d_6 (Figure S6) solvents, aliphatic proton peaks appeared in the upfield region between δ 1.18 and 3.46. The aromatic protons peaks were observed in the downfield region at δ 7.47−8.26. The chemical shift of the C_{12} proton DMSO-d_6 is in the range of δ 7.75; however, in $CDCl_3$, it is at about δ 7.59. The C_{13} proton in DMSO-d_6 as a multiplet appeared in the range of δ 7.89−7.95 but in $CDCl_3$ at δ 7.78. The C_{18} aliphatic proton showed in $CDCl_3$ at δ 1.30 but in DMSO-d_6 at δ 1.18 due to the solvent polarity. The ^{13}C NMR spectrum shows the presence of 18 carbons. The characteristic signals at δ 203.29 and δ 202.51 were due to $-C_{16}{=}O$ using $CDCl_3$ (Figure S10) and DMSO-d_6 (Figure S11) solvents,

https://doi.org/10.1021/acsomega.3c04360
ACS Omega 2023, 8, 43573−43585

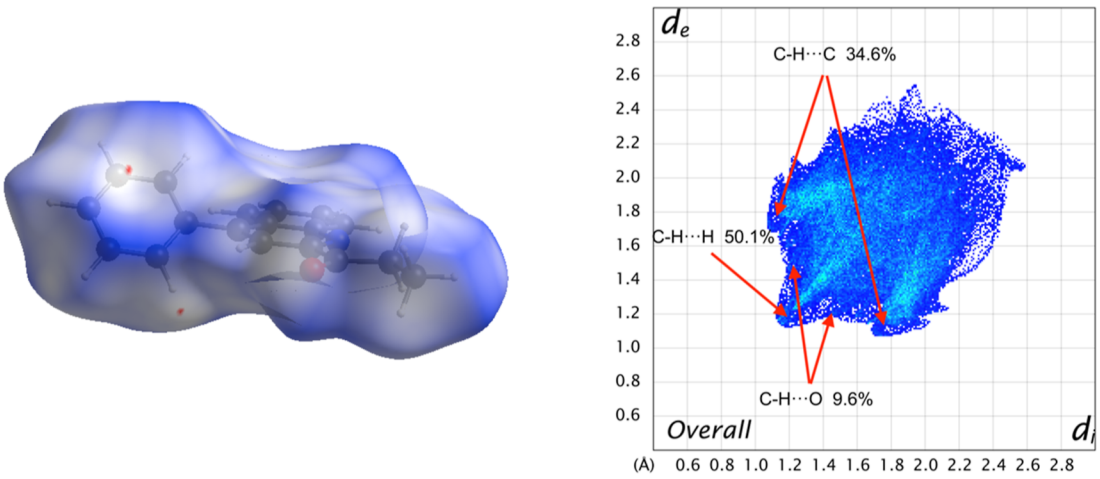

Figure 7. d_{norm} surface for molecule **3** (left) and its overall 2D fingerprint plot (right), indicating the most important contacts in the crystal packing. Red and blue colors indicate strong and weak interactions, respectively. Isovalues range from −0.0051 (red) to +1.3934 (blue).

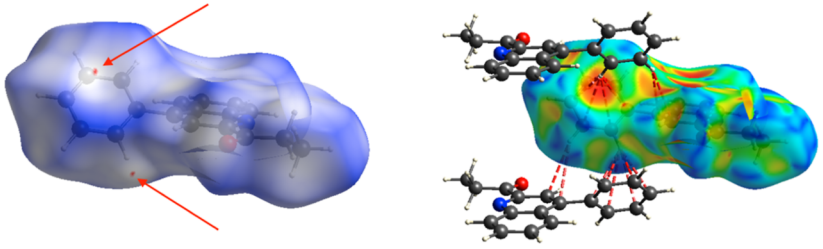

Figure 8. d_{norm} surface for molecule **3** (left) and its shape index plot (right) indicate the C−H···π contacts in the crystal packing. Isovalues range from −0.0051 (red/orange) to +1.3934 (blue).

respectively. The characteristic signals in the aliphatic region at δ 8.14 (C_{18}), 30.91 (C_{17}) and δ 8.42 (C_{18}), 30.72 (C_{17}) appeared using $CDCl_3$ (Figure S10) and DMSO-d_6 (Figure S11) solvents, respectively. All other aromatic carbons appeared in the region of δ 118.09−152.64. From DEPT-135 spectra, 30.91 (C_{17}) and 30.72 (C_{17}) were shown in $CDCl_3$ (Figure S15) and DMSO-d_6 (Figure S16) solvents, respectively, which is identified in the downfield region due to the even number of protons.

The ^{1}H and ^{13}C NMR spectra of molecule **3** were calculated by using B3LYP/6-311G(d,p), CAM-B3LYP/6-311G(d,p), and M06-2X/6-311G(d,p) levels of density functional calculations, and experimental chemical shift values are represented as a distribution graph in Figure 3. The theoretical ^{1}H and ^{13}C chemical shift values compared with experimental ^{1}H and ^{13}C chemical shift values showed in Tables 2 and 3. The theoretical ^{1}H and ^{13}C chemical shift results for (**3**) are mostly closer to the experimental ^{1}H and ^{13}C shift data. The optimized electronic structure (Figure 1), FT-IR (Figures S2−S4), and NMR (Figures S7−S9 and S12−S14) spectroscopy of molecule **3** were performed using at B3LYP/6-311G(d,p), CAM-B3LYP/6-311G(d,p), and M06-2X/6-311G(d,p) levels of theory. The absence of imaginary frequencies for the optimized geometry of molecule **3** suggests a suitable conversion of the model calculations.

4.2.4. Single-Crystal XRD Studies. 4.2.4.1. Crystal and Molecular Structure. The molecular structure of 1-(4-phenylquinolin-2-yl)propan-1-one (**3**) crystallizes in a orthorhombic system, in the space group $P2_12_12_1$ (Z = 4), with normal bond angles and distances[62] and similar to related compounds.[63,64] The fragments linked to the quinoline ring are practically planar, except for phenyl ring attached to quinoline ring, were their mean planes have a torsion angle of 49.5(1)°, in agreement with 56.75(8) and 61.35(6) found in other similar compounds[63,64] (see Figure 4 for more details). A summary of the details about crystal data, collection parameters, and refinement is included in Table 4, and additional crystallographic details are included in the CIF files. ORTEP (Figure 4) views were drawn using OLEX2 software.[45]

The calculated geometrical parameters (bond length, bond angle, and dihedral angle) of molecule **3** and single-crystal X-ray diffraction (XRD) data are listed in Table 5, following the atom numbering scheme given in Figure 1.

The distribution graphs show the agreement between calculated and experimental structural parameters. Correlation coefficients (R^2) are 0.9827, 0.9794, and 0.9973 for bond length, bond angles, and dihedral, respectively, in Figure 5. According to Table 5 and Figure 5, the calculated and experimental values of geometrical parameters were satisfactory.

4.2.5. Noncovalent Interactions. Additionally, the crystal structure does not show classic hydrogen bonds between neighbor molecules. However, one C−H···O intermolecular bifurcated hydrogen bond interaction is observed with graph-set notation $\mathbf{C_1^1(8)}$, $\mathbf{C_1^1(9)}$, and $\mathbf{R_1^2(5)}$.[65] Large C−H···π interactions are also observed in the crystal structure of the title compound. Both interactions observed in the crystal structure lie in each screw axis present in the space group. Moreover, the distances between involved atoms is larger than the sum of the VdW radii[60,61] (see Figure 6 and Table 6 for more details).

https://doi.org/10.1021/acsomega.3c04360
ACS Omega 2023, 8, 43573−43585

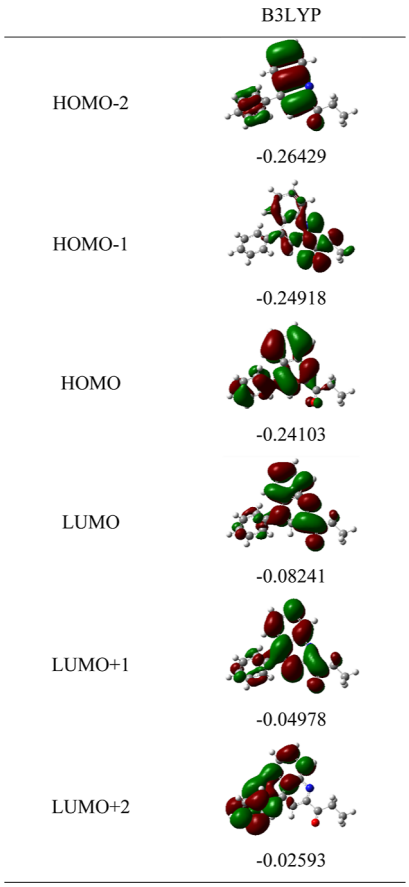

Figure 9. Molecular orbital (MO) energy diagrams (eV) from HOMO − 2 to LUMO + 2 at B3LYP/6-311G(d,p) molecule **3** in the gas phase.

4.2.6. Hirshfeld Surface Analyses. Hirshfeld surface analysis was utilized as a complementary analysis for the crystal packing contacts. The intermolecular interactions are mainly constituted by C−H···O, which are shown as red (d_{norm} < VdW radii), white (d_{norm} = VdW radii), and blue (d_{norm} > VdW radius) spots in the d_{norm} surfaces for all compounds. Furthermore, there is evidence of some other interesting weak contacts with less impact on the crystal structure, such as C−H···π contacts. The reciprocal contacts and their corresponding contributions are displayed in Figure 7 and all fingerprint plots with d_{norm} (where $d_{norm} = d_i + d_e$) surfaces for their intermolecular contacts were calculated at the BLYP/6-31G(d,p) level of theory in the cluster of radius 3.8 Å around the molecule.[57]

The reciprocal contacts for C−H···O appear as a wide symmetrical wing with $d_e + d_i \sim 2.7$, corresponding to classical hydrogen bond interactions. However, this is larger than the sum of the VdW radii, as mentioned above. In the case of C−H···N interactions, the distance is slightly higher than the VdW radii for N and H atoms ($d_e + d_i > 2.75$ Å),[61] where the contribution is negligible. Remarkably, The interatomic contacts of C−H···H interactions display a $d_i + d_e \sim 2.4$ Å = 2.4 Å, with a contribution of around 50.1%, creating a nonsignificant effect over molecular packing in the crystal structure stabilization, in other words, these contacts are slightly larger than the sum of the VdW radii for these atoms.[60,61]

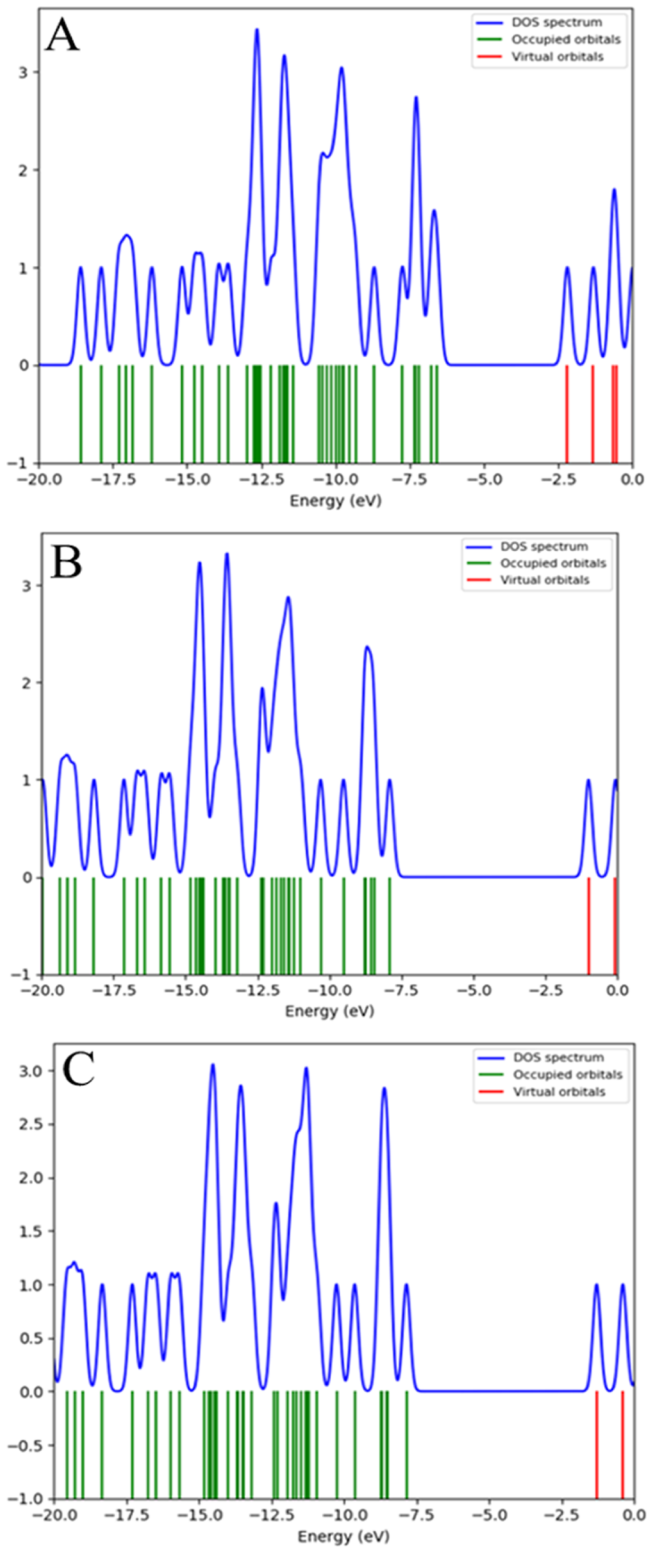

Figure 10. Simulated density of states spectrum of molecule **3** with (A) B3LYP/6-311G(d,p), (B) CAM-B3LYP/6-311G(d,p), and (C) M06-2X/6-311G(d,p) levels of theory.

In the Hirshfeld surface analysis, there is another type of weak interactions. For example, the contribution of H···π type interaction is around 34.6%, when $d_e + d_i$ of ∼2.9 Å. This was analyzed with a shape index, allowing us to determine the presence of these weak interactions. The yellow-orange spots exhibit surface subsidence due to the proximity of the

https://doi.org/10.1021/acsomega.3c04360
ACS Omega 2023, 8, 43573−43585

Table 7. FMO Energies, Chemical Potential (μ), Hardness (η) Softness (S), and Electronegativity (χ) Parameters for the Molecule 3 Calculated with B3LYP/6-311G(d,p), CAM-B3LYP/6-311G(d,p), and M06-2X/6-311G(d,p) Levels of Theory

property	B3LYP/6-311G(d,p)	CAM-B3LYP/6-311G(d,p)	M06-2X/6-311G(d,p)
E_{HOMO}	−0.24103	−0.29054	−0.28706
E_{LUMO}	−0.08241	−0.03665	−0.04792
E_{GAP}	0.15862	0.25389	0.23914
chemical potential (μ)	−0.16172	−0.16359	−0.16749
global hardness (η)	0.07931	0.12695	0.11957
global softness (S)	6.30437	3.93856	4.18165
global electronegativity (χ)	0.16172	0.16359	0.16749

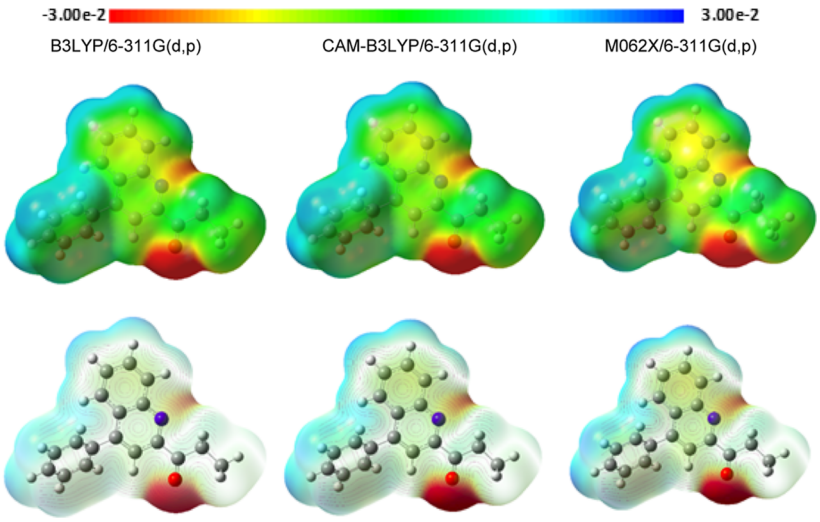

Figure 11. MEP maps and contours of molecule **3** at B3LYP/6-311G(d,p), CAM-B3LYP/6-311G(d,p), and M06-2X/6-311G(d,p) levels in the gas phase.

neighboring moieties and the blue-green spots demonstrate the reciprocal contacts of the moieties that generate the subsidence.

In this context, their corresponding counterparts, where the interaction between hydrogens and delocalized π-clouds bonds are demonstrated when constructing the crystal structure, are shown in Figure 8. However, the sum of VdW radii for C and H atoms interacting between them is slightly larger than their theoretical value (2.95 vs 2.9 Å).[60,61] Thus, these types of interactions can be reflected weakly as for the d_{norm} surface.

4.2.7. Frontier Molecular Orbitals, MEP Maps, and MEP Contours. The DFT calculations of MOs and their energy diagrams were executed at the B3LYP/6-311G(d,p), CAM-B3LYP/6-311G(d,p), and M06-2X/6-311G(d,p) levels of theory in the gas phase. Frontier molecular orbitals (FMOs), such as the HOMO and the LUMO, were exploited to determine the chemical reactivity. The distributions of the energy diagrams from HOMO − 2 to LUMO + 2 for molecule **3** are given in Figure 9 at the B3LYP/6-311G(d,p) level. The results at other calculation levels are listed in Figure S19 (Supporting Information). It is noticed that electrons in HOMO are mostly localized on the quinoline ring of molecule **3**. The presence of electrons in LUMO is also located in the same region of the quinoline ring, indicating the presence of increased chemical activity. The values of hardness, softness, chemical potential, and electronegativity for molecule **3** in the gas phase with B3LYP/6-311G(d,p), CAM-B3LYP/6-311G-(d,p), and M06-2X/6-311G(d,p) levels of theory basis sets. In this report, the character of the MOs is calculated using the same levels of theory, and the density of the states (DOS) is shown in Figure 10. DOS plot exhibits the MO compositions at the different energy levels of molecule **3**. Moreover, the DOS is also notable for numerous calculations, such as estimating the occupancy of states and virtual orbitals of molecule **3** using red and green lines in the spectrum.[66,67] The mentioned quantum chemical parameters are calculated using eqs 1−5 and are given in Table 7.

According to Table 7, selected quantum chemical calculations are close to each other in the CAM-B3LYP/6-311G(d,p) and M06-2X/6-311G(d,p) levels. The results in B3LYP/6-311G(d,p) are different from other. However, these results do not represent any errors. When the result of this study is comparable to previous reports,[68] it is observed that the spherical softness of the studied molecule is quite large at each computational level, and it is lower in the energy gap. In this case, it states that the studied molecule can easily interact.

MEP maps are correlated to electron density on molecular surfaces. These maps can be depicted in nucleophilic or electrophilic active zones. MEP maps and contours of molecule **3** at B3LYP/6-311G(d,p), CAM-B3LYP/6-311G-(d,p), and M06-2X/6-311G(d,p) levels in the gas phase are represented in Figure 11. In the MEP contour map, the negative regions (designated as red) of MEP are related to electrophilic attacks, and positive regions (designated as blue) are related to nucleophilic reactivity. According to MEP maps in Figure 11, the environment of the oxygen atom in the carbonyl group with red color acts at the electrophilic reactive site. The surfaces around the nitrogen atom are blue color, which can act as a nucleophilic reactive site.

https://doi.org/10.1021/acsomega.3c04360
ACS Omega 2023, 8, 43573−43585

Table 8. NBO Atomic Charges (e) of the Molecule 3

atom	B3LYP	CAM-B3LYP	M06-2X
C1	−0.058	−0.060	−0.064
C2	−0.186	−0.190	−0.192
C3	−0.192	−0.194	−0.196
C4	−0.194	−0.200	−0.201
C5	−0.194	−0.197	−0.199
C6	−0.194	−0.199	−0.201
C7	0.018	0.023	0.018
C8	−0.200	−0.210	−0.212
C9	0.126	0.130	0.131
C10	0.164	0.162	0.163
C11	−0.171	−0.176	−0.177
C12	−0.192	−0.197	−0.199
C13	−0.184	−0.188	−0.190
C14	−0.187	−0.191	−0.194
C15	−0.067	−0.069	−0.073
C16	0.538	0.550	0.550
C17	−0.464	−0.475	−0.481
C18	−0.569	−0.582	−0.583
N1	−0.439	−0.440	−0.433
O1	−0.548	−0.552	−0.549
H2	0.212	0.216	0.219
H3	0.207	0.211	0.213
H4	0.205	0.209	0.212
H5	0.206	0.210	0.213
H6	0.212	0.216	0.219
H8	0.240	0.246	0.248
H11	0.220	0.224	0.227
H12	0.208	0.212	0.214
H13	0.207	0.211	0.213
H14	0.219	0.223	0.226
H17a	0.229	0.233	0.236
H17b	0.229	0.234	0.236
H18a	0.202	0.206	0.207
H18b	0.195	0.199	0.201
H18c	0.201	0.206	0.207

4.2.8. Thermodynamics Parameters. The thermodynamic parameters of molecule **3** have been calculated to get reliable relations among energetic, structural, and reactivity characteristics of the molecules. Table S3 (Supporting Information) shows the values of thermodynamic parameters such as, Gibbs free energy, entropy allows us to estimate the stability of the compound, and zero-point energy gives information about the nuclear motion of the structure.[69]

4.2.9. NBO Charges. Our interest is to compare the different methods to describe the distribution of electrons in the compound under study and evaluating the sensitivity of the calculated charges to changes in the quantum mechanical method used. The N(1) and the O(1) atoms have the highest negative charges. These charges, being relatively close in space, make this fragment of the molecule a potential coordination site with metal ions. Natural bond orbital (NBO) charges of atoms in studied compound are calculated at each calculation level and given in Table 8.

It is interesting to notice that the dipole moment is higher for B3LYP calculation compared with CAM-B3LYP and M06-2X methods. Therefore, B3LYP describes a more polarized structure than the other DFT methods.

4.2.10. Determination of NLO Properties. We carried out the study to calculate the dipolar moment (u) linear polarizability (α) and the first order hyperpolarizability (β) using the B3LYP, CAM-B3LYP, and M06-2X functional with the 6-311G(d,p) basis set in the gas phase. These parameters are important to predict the NLO properties of molecules for their potential application in optoelectronic technologies in the field of telecommunications, signal processing, data storage, microscopy to higher harmonic, etc.[70] For its part, urea is a reference substance for NLO material for comparative purposes.[71,72] Table 9 shows the dipole moments and static electronic polarizabilities of molecule **3** obtained from the calculated parameters.

Interestingly, even though both molecule **3** and urea have relatively similar dipole moments, the linear polarizability and hyperpolarizability of molecule **3** are approximately 5 times higher compared to urea. Thus, the large magnitude of $\langle\alpha\rangle$ and β_{total} indicate that the molecule **3** is highly polarizable; therefore, this molecule **3** could potentially serve as NLO material.

5. CONCLUSIONS

In the present work, PPA-assisted synthesis of a novel 1-(4-phenylquinolin-2-yl)propan-1-one from 2-aminobenzophenone and pentan-2,3-dione under solvent-free Friedländer quinoline synthesis is shown. The synthesized 1-(4-phenylquinolin-2-yl)propan-1-one (**3**) is confirmed by molecular and structural analysis like FT-IR, ^{1}H and ^{13}C NMR chemical shifts, and single-crystal XRD techniques. DFT calculations for

Table 9. Dipole Moments and Static Electronic Polarizabilities of the Molecule 3 Calculated with B3LYP/6-311G(d,p), CAM-B3LYP/6-311G(d,p), and M06-2X/6-311G(d,p) Levels of Theory

property	urea			molecule 3		
	B3LYP	CAM-B3LYP	M06-2X	B3LYP	CAM-B3LYP	M06-2X
μ_x	0.0012	0.0014	0.0000	−2.5628	−2.5084	−2.4506
μ_y	−3.6204	−3.6204	−3.6049	2.2797	2.2452	2.2356
μ_z	0.0004	0.0001	0.0000	−0.0981	−0.0957	−0.0983
μ[a]	3.6204	3.6964	3.6049	3.4314	3.3678	3.3186
α_{xx}	−17.4265	−17.3455	−17.4046	−106.5586	−106.1839	−104.7016
α_{yy}	−24.9745	−24.978	−25.0079	−114.7163	−114.8909	−113.9694
α_{zz}	−24.9976	−25.0503	−25.0713	−115.7369	−116.0649	−116.3475
$\langle\alpha\rangle$[b]	−22.2697	−22.2333	−22.2696	−112.3373	−112.3799	−111.6728
$(\Delta\alpha)$[b]	8.9713	8.9686	9.1274	15.9477	16.40179	17.2993
β_{total}[c]	11.9617	12.3879	11.9143	57.6441	57.3569	55.5248

[a]In Debye. [b]In ($\times 10^{-23}$) esu. [c]In ($\times 10^{-30}$) esu.

https://doi.org/10.1021/acsomega.3c04360
ACS Omega 2023, 8, 43573−43585

molecule **3** were measured and calculated using B3LYP/6-311G(d,p), CAM-B3LYP/6-311G(d,p), and M06-2X/6-311G(d,p) basis sets in the gas phase. As a result, it has been found that there is a good correlation between calculated and experimental data. The optimized geometry of the quinoline molecule was compared with the experimental XRD values. DFT calculations of the noncovalent interactions, Hirshfeld surface analysis, NLO properties, thermodynamic properties, and FMO acknowledged chemically active sites of the quinoline compound accountable for its chemical reactivity. The MEP results showed that the most reactive site for any nucleophilic attack is the nitrogen atom, while the most reactive site for any electrophilic attack is the oxygen atom. These findings may provide information about potential reactive regions on the whole molecule. It is interesting to observe that the dipole moment is higher for B3LYP calculation than for CAM-B3LYP and M06-2X methods. Therefore, B3LYP describes a more polarized structure than the other DFT methods.

■ ASSOCIATED CONTENT

Supporting Information

The Supporting Information is available free of charge at https://pubs.acs.org/doi/10.1021/acsomega.3c04360.

General procedure for synthesis, spectral data, and theoretical investigation of molecule **3** (PDF)

The Cambridge Crystallographic Data Centre has deposited CIF files for compound **3** with the CCDC number 2077085. Copies of the data can be obtained, free of charge, on application to CCDC, 12 Union Road, Cambridge, CB2 1EZ, UK. Fax: +44 (0) 1223 336033 or Email: deposit@ccdc.cam.ac.uk (CIF)

■ AUTHOR INFORMATION

Corresponding Authors

Satheeshkumar Rajendran − *Departamento de Química Orgánica, Facultad de Química y de Farmacia, Pontificia Universidad Católica de Chile, 702843 Santiago de Chile, Chile; Department of Pharmaceutical Sciences, Irma Lerma Rangel School of Pharmacy, Texas A&M Health Science Center, Texas A&M University, Kingsville, Texas 78363, United States;* orcid.org/0000-0001-8492-286X; Email: drrsatheeshphd@gmail.com

Nitin Bharat Charbe − *Center for Pharmacometrics and Systems Pharmacology, Department of Pharmaceutics, College of Pharmacy, University of Florida, Orlando, Florida 32611, United States*; Email: nitin.charbe@ufl.edu

Murtaza M. Tambuwala − *Lincoln Medical School, University of Lincoln, Lincoln LN6 7TS, U.K.;* orcid.org/0000-0001-8499-9891; Email: mtambuwala@lincoln.ac.uk

Authors

Rodrigo Montecinos − *Departamento de Química Física, Facultad de Química y de Farmacia, Pontificia Universidad Católica de Chile, 702843 Santiago de Chile, Chile;* orcid.org/0000-0003-0080-1839

Jonathan Cisterna − *Departamento de Química, Facultad de Ciencias Básicas, Universidad de Antofagasta, Antofagasta 1240000, Chile;* orcid.org/0000-0001-5952-7083

Kolandaivel Prabha − *Department of Chemistry, K. S. Rangasamy College of Technology, Tiruchengode 637215 Tamil Nadu, India*

Karnam Jayarampillai Rajendra Prasad − *Department of Chemistry, Bharathiar University, Coimbatore 641046, India*

Sushesh Srivatsa Palakurthi − *Department of Pharmaceutical Sciences, Irma Lerma Rangel School of Pharmacy, Texas A&M Health Science Center, Texas A&M University, Kingsville, Texas 78363, United States*

Alaa A. A Aljabali − *Department of Pharmaceutical Sciences, Faculty of Pharmacy, Yarmouk University, Irbid 566, Jordan;* orcid.org/0000-0002-9519-6338

Gowhar A. Naikoo − *Department of Mathematics & Sciences, College of Arts & Applied Sciences, Dhofar University, Salalah 211, Oman*

Vijay Mishra − *School of Pharmaceutical Sciences, Lovely Professional University, Phagwara, Punjab 144411, India*

Roberto Acevedo − *Facultad de Ingeniería y Tecnología, Universidad San Sebastián, Santiago 8420524, Chile*

Koray Sayin − *Department of Chemistry, Faculty of Science, Sivas Cumhuriyet University, Sivas 58140, Turkey;* orcid.org/0000-0001-6648-5010

Complete contact information is available at: https://pubs.acs.org/10.1021/acsomega.3c04360

Author Contributions

Rajendran Satheeshkumar: conceptualization, methodology, and writing—original draft preparation; **Rodrigo Montecinos:** data curation and original draft preparation; **Jonathan Cisterna, Kolandaivel Prabha, Nitin Bharat Charbe,** and **Sushesh Palakurthi:** reviewing and editing; **Roberto Acevedo** and **Karnam Jayarampillai Rajendra Prasad:** reviewing and editing; and **Koray Sayin** and **Murtuza Tambuwala**: data curation and reviewing and editing.

Author Contributions

All the data out from software have been included in the paper.

Funding

Consent for publication: All authors gave consent for publication.

Notes

The authors declare no competing financial interest.

■ ACKNOWLEDGMENTS

S.R. is thankful to the financial support of FONDECYT for a Postdoctoral (Project no. 3190292) fellowship and Dr. Cristian Salas, Faculty of Chemistry and Pharmacy, Pontificia Universidad Católica de Chile, Chile, which are gratefully acknowledged. The authors also acknowledge Dr. Iván Brito, Facultad de Ciencias Básicas, Universidad de Antofagasta, Antofagasta, Chile and Dr. Werner Kaminsky, Department of Chemistry, University of Washington, Seattle, WA 98195, USA, for single-crystal XRD analysis.

■ REFERENCES

(1) Nainwal, L. M.; Tasneem, S.; Akhtar, W.; Verma, G.; Khan, M. F.; Parvez, S.; Shaquiquzzaman, M.; Akhter, M.; Alam, M. M. Green Recipes to Quinoline: A Review. *Eur. J. Med. Chem.* **2019**, *164*, 121−170.

(2) Morimoto, Y.; Matsuda, F.; Shirahama, H. Total Synthesis of (±)-Virantmycin and Determination of Its Stereochemistry. *Synlett* **1991**, *1991* (03), 202−203.

(3) Michael, J. P. Quinoline, Quinazoline and Acridone Alkaloids. *Nat. Prod. Rep.* **1997**, *14* (6), 605−618.

(4) Michael, J. P. Quinoline, Quinazoline and Acridone Alkaloids. *Nat. Prod. Rep.* **2002**, *19* (6), 742−760.
(5) Markees, D. G.; Dewey, V. C.; Kidder, G. W. Antiprotozoal 4-Aryloxy-2-Aminoquinolines and Related Compounds. *J. Med. Chem.* **1970**, *13* (2), 324−326.
(6) Campbell, S. F.; Hardstone, J. D.; Palmer, M. J. 2,4-Diamino-6,7-dimethoxyquinoline Derivatives as .alpha.1-Adrenoceptor Antagonists and Antihypertensive Agents. *J. Med. Chem.* **1988**, *31* (5), 1031−1035.
(7) Yadav, P.; Shah, K. Quinolines, a Perpetual, Multipurpose Scaffold in Medicinal Chemistry. *Bioorg. Chem.* **2021**, *109*, 104639.
(8) Kaur, R.; Kumar, K. Synthetic and Medicinal Perspective of Quinolines as Antiviral Agents. *Eur. J. Med. Chem.* **2021**, *215*, 113220.
(9) Skraup, Z. H. Eine Synthese Des Chinolins. *Monatsh. Chem.* **1880**, *1* (1), 316−318.
(10) Li, J. J. Skraup Quinoline Synthesis. In *Name Reactions*; Springer, 2003; pp 378−379.
(11) Doebner, O.; von Miller, W. Ueber Eine Dem Chinolin Homologe Base. *Ber. Dtsch. Chem. Ges.* **1881**, *14* (2), 2812−2817.
(12) Pfitzinger, W. Chinolinderivate Aus Isatinsäure. *J. Prakt. Chem.* **1885**, *33* (1), 100.
(13) Conrad, M.; Limpach, L. Synthesen von Chinolinderivaten Mittelst Acetessigester. *Ber. Dtsch. Chem. Ges.* **1887**, *20* (1), 944−948.
(14) Surrey, A. R. *Combes Quinoline Synthesis*, 2nd ed.; Academic Press Inc., 1961..
(15) Povarov, L. S. *αβ*-Unsaturated Ethers and their Analogues in Reactions of Diene Synthesis. *Russ. Chem. Rev.* **1967**, *36* (9), 656−670.
(16) Povarov, L. S. Reactions of Acetals With Unsaturated Ethers. *Russ. Chem. Rev.* **1965**, *34* (9), 639−656.
(17) Cheng, C.-C.; Yan, S.-J. The Friedländer Synthesis of Quinolines. *Org. React.* **1982**, *17*, 37−201.
(18) Friedländer, P.; Gohring, C. F. Ueber Eine Darstellungsmethode Im Pyridinkern Substituirter Chinolinderivate. *Ber. Dtsch. Chem. Ges.* **1883**, *16* (2), 1833−1839.
(19) Rajendran, S.; Sivalingam, K.; Karnam Jayarampillai, R. P.; Wang, W.-L. L.; Salas, C. O. Friedländer's Synthesis of Quinolines as a Pivotal Step in the Development of Bioactive Heterocyclic Derivatives in the Current Era of Medicinal Chemistry. *Chem. Biol. Drug Des.* **2022**, *100* (6), 1042−1085.
(20) Marco-Contelles, J.; Pérez-Mayoral, E.; Samadi, A.; Carreiras, M. D. C.; Soriano, E. Recent Advances in the Friedländer Reaction. *Chem. Rev.* **2009**, *109* (6), 2652−2671.
(21) Shiri, M.; Zolfigol, M. A.; Kruger, H. G.; Tanbakouchian, Z. *Friedländer Annulation in the Synthesis of Azaheterocyclic Compounds*; Academic Press, 2011; Vol. *102*..
(22) Li, J. J. Friedländer Quinoline Synthesis. In *Name Reactions*; Springer, 2021; pp 206−208..
(23) Ghobadi, N.; Nazari, N.; Gholamzadeh, P. The Friedländer Reaction: A Powerful Strategy for the Synthesis of Heterocycles. *Adv. Heterocycl. Chem.* **2020**, *132*, 85−134.
(24) Satheeshkumar, R.; Rajendra Prasad, K. J. Solvent-Free Synthesis of Dibenzo[b,j] [1,10]Phenanthroline Derivatives Using Eaton's Reagent as Catalyst. *Synth. Commun.* **2017**, *47* (10), 990−998.
(25) Satheeshkumar, R.; Shankar, R.; Kaminsky, W.; Rajendra Prasad, K. J. Novel Synthetic and Mechanistic Approach of TFA Catalysed Friedländer Synthesis of 2-Acylquinolines from Symmetrical and Unsymmetrical 1,2-Diketones with o-Aminoarylketones. *ChemistrySelect* **2016**, *1* (21), 6823−6829.
(26) Satheeshkumar, R.; Sayin, K.; Kaminsky, W.; Rajendra Prasad, K. J. Indium Triflate and Ionic Liquid-Mediated Friedländer Synthesis of 2-Acylquinolines. *Synth. Commun.* **2017**, *47* (21), 1940−1954.
(27) Satheeshkumar, R.; Kaminsky, W.; Sparkes, H. A.; Rajendra Prasad, K. J. Efficient Protocol for Synthesis of Pyrazolo[3,4-a]Acridines. *Synth. Commun.* **2015**, *45* (19), 2203−2215.
(28) Satheeshkumar, R.; Kaminsky, W.; Rajendra Prasad, K. J. Efficient Novel Synthesis of Pyrano[3,2-a]- and Pyrazolo[4,3-a]-Acridines. *Synth. Commun.* **2017**, *47* (3), 245−255.
(29) Satheeshkumar, R.; Shanmugaraj, K.; Delgado, T.; Bertrand, J.; Brito, I.; Salas, C. O. Friedländer Synthesis of Novel Polycyclic Quinolines Using Solid SiO_2/H_2SO_4 Catalyst. *Org. Prep. Proced. Int.* **2021**, *53* (2), 138−144.
(30) Hasaninejad, A.; Zare, A.; Shekouhy, M.; Ameri-Rad, J. Sulfuric Acid-Modified PEG-6000 (PEG-OSO3H): An Efficient, Bio-Degradable and Reusable Polymeric Catalyst for the Solvent-Free Synthesis of Poly-Substituted Quinolines under Microwave Irradiation. *Green Chem.* **2011**, *13* (4), 958−964.
(31) McAteer, C. H.; Murugan, R.; Subba Rao, Y. V. *Heterogeneously Catalyzed Synthesis of Heterocyclic Compounds*; Academic Press, 2017; Vol. *121*..
(32) Satheeshkumar, R.; Shankar, R.; Kaminsky, W.; Kalaiselvi, S.; Padma, V. V.; Rajendra Prasad, K. J. Theoretical and Experimental Investigations on Molecular Structure of 7-Chloro-9-Phenyl-2,3-Dihydroacridin-4(1H)-One with Cytotoxic Studies. *J. Mol. Struct.* **2016**, *1109*, 247−257.
(33) Satheeshkumar, R.; Sayin, K.; Kaminsky, W.; Rajendra Prasad, K. J. Synthesis, Spectral Analysis and Quantum Chemical Studies on Molecular Geometry, Chemical Reactivity of 7-Chloro-9-(2′-Chlorophenyl)-2,3-Dihydroacridin-4(1H)-One and 7-Chloro-9-(2′-Fluorophenyl)-2,3-Dihydroacridin-4(1H)-One. *J. Mol. Struct.* **2017**, *1128*, 279−289.
(34) Satheeshkumar, R.; Rajamanikandan, R.; Ilanchelian, M.; Sayin, K.; Prasad, K. J. R. Synthesis of Novel 1,10-Phenanthroline Derivatives and It Used as Probes for Sensitive Detection of Zn^{2+} and Cd^{2+} Metal Ions—Spectroscopic and Theoretical Approach. *Spectrochim. Acta, Part A* **2019**, *221*, 117196.
(35) Satheeshkumar, R.; Sayin, K.; Kaminsky, W.; Rajendra Prasad, K. J. Synthesis, Spectroscopic, In Vitro Cytotoxicity and Crystal Structures of Novel Fluorinated Dispiroheterocycles: DFT Approach. *Monatsh. Chem.* **2018**, *149* (1), 141−147.
(36) Jayarajan, R.; Satheeshkumar, R.; Kottha, T.; Subbaramanian, S.; Sayin, K.; Vasuki, G. Water Mediated Synthesis of 6-Amino-5-cyano-2-oxo-N-(pyridin-2-yl)-4-(p-tolyl)-2H-[1,2′-bipyridine]-3-carboxamide and 6-amino-5-cyano-4-(4-fluorophenyl)-2-oxo-N-(pyridin-2-yl)-2H-[1,2′-bipyridine]-3-carboxamide—An Experimental and Computational Studies with Non-Linear Optical (NLO) and Molecular Docking Analyses. *Spectrochim. Acta, Part A* **2020**, *229*, 117861.
(37) Satheeshkumar, R.; Prabha, K.; Vennila, K. N.; Sayin, K.; Güney, E.; Kaminsky, W.; Acevedo, R. Spectroscopic (FT-IR, NMR, Single Crystal XRD) and DFT Studies Including FMO, Mulliken Charges, and Hirshfeld Surface Analysis, Molecular Docking and ADME Analyses of 2-Amino-4′-Fluorobenzophenone (FAB). *J. Mol. Struct.* **2022**, *1267*, 133552.
(38) Popp, F. D.; Mcewen, W. E. Polyphosphoric Acids As A Reagent In Organic Chemistry. *Chem. Rev.* **1958**, *58* (2), 321−401.
(39) So, Y. H.; Heeschen, J. P. Mechanism of Polyphosphoric Acid and Phosphorus Pentoxide-Methanesulfonic Acid as Synthetic Reagents for Benzoxazole Formation. *J. Org. Chem.* **1997**, *62* (11), 3552−3561.
(40) Prabha, K.; Satheeshkumar, R.; Rajendra Prasad, K. J. Synthesis and Cytotoxicity of Novel Indoloquinolines and Benzonaphthyridines from 4-Chloro-2,8-Dimethylquinoline and Variety of Hetero Amines. *ChemistrySelect* **2021**, *6* (28), 7136−7142.
(41) Kolandaivel, P.; Rajendran, S.; Karnam Jayarampillai, R. P. Synthesis of Novel Benzo Naphtho Naphthyridines from 2,4-Dicloroquinolines. *J. Heterocycl. Chem.* **2021**, *58* (9), 1809−1824.
(42) Bruker AXS Inc. *APEX3 Package*, APEX3, SAINT and SADABS; Bruker AXS Inc.: Madison, Wisconsin, USA, 2016.
(43) Sheldrick, G. M. *SADABS*, Software for Empirical Absorption Correction; University of Göttingen: Germany, 2000.
(44) Sheldrick, G. M. Crystal Structure Refinement with SHELXL. *Acta Crystallogr., Sect. C: Struct. Chem.* **2015**, *71* (1), 3−8.

https://doi.org/10.1021/acsomega.3c04360
ACS Omega 2023, 8, 43573−43585

(45) Dolomanov, O. V.; Bourhis, L. J.; Gildea, R. J.; Howard, J. A. K.; Puschmann, H. OLEX2 : A Complete Structure Solution, Refinement and Analysis Program. *J. Appl. Crystallogr.* **2009**, *42* (2), 339−341.
(46) Becke, A. D. Density-Functional Thermochemistry. III. The Role of Exact Exchange. *J. Chem. Phys.* **1993**, *98* (7), 5648−5652.
(47) Yanai, T.; Tew, D. P.; Handy, N. C. A New Hybrid Exchange-Correlation Functional Using the Coulomb-Attenuating Method (CAM-B3LYP). *Chem. Phys. Lett.* **2004**, *393* (1−3), 51−57.
(48) Zhao, Y.; Truhlar, D. G. The M06 Suite of Density Functionals for Main Group Thermochemistry, Thermochemical Kinetics, Noncovalent Interactions, Excited States, and Transition Elements: Two New Functionals and Systematic Testing of Four M06-Class Functionals and 12 Other Functionals. *Theor. Chem. Acc.* **2008**, *120* (1−3), 215−241.
(49) Krishnan, R.; Binkley, J. S.; Seeger, R.; Pople, J. A. Self-consistent Molecular Orbital Methods. XX. A Basis Set for Correlated Wave Functions. *J. Chem. Phys.* **1980**, *72* (1), 650−654.
(50) Dennington, R.; Todd Keith, J. M. *GaussView*, Version 5, 2009.
(51) Frisch, M. J.; Trucks, G. W.; Schlegel, H. B.; Scuseria, G. E.; Robb, M. A.; Cheeseman, J. R.; Scalmani, G.; Barone, V.; Mennucci, B.; Petersson, G. A.; Nakatsuji, H.; Caricato, M.; Li, X.; Hratchian, H. P.; Izmaylov, A. F.; Bloino, J.; Zheng, G.; Sonnenb, D. J. *Gaussian 09*, Revision A.02, 2009.
(52) PerkinElmer. *ChemBioDraw Ultra*, Version (13.0.0.3015); CambridgeSoftWaltham: MA, USA, 2012.
(53) Kohn, W.; Sham, L. J. Quantum Density Oscillations in an Inhomogeneous Electron Gas. *Phys. Rev.* **1965**, *137* (6A), A1697−A1705.
(54) Jesudason, E. P.; Sridhar, S. K.; Malar, E. P.; Shanmugapandiyan, P.; Inayathullah, M.; Arul, V.; Selvaraj, D.; Jayakumar, R. Synthesis, Pharmacological Screening, Quantum Chemical and In Vitro Permeability Studies of N-Mannich Bases of Benzimidazoles through Bovine Cornea. *Eur. J. Med. Chem.* **2009**, *44* (5), 2307−2312.
(55) Gökce, H.; Bahçeli, S. A Study on Quantum Chemical Calculations of 3-4-Nitrobenzaldehyde Oximes. *Spectrochim. Acta, Part A* **2011**, *79* (5), 1783−1793.
(56) McKinnon, J. J.; Jayatilaka, D.; Spackman, M. A. Towards Quantitative Analysis of Intermolecular Interactions with Hirshfeld Surfaces. *Chem. Commun.* **2007**, No. 37, 3814−3816.
(57) Wolff, S. K.; Grimwood, D. J.; McKinnon, J. J.; Turner, M. J.; Jayatilaka, D.; Spackman, M. A. *Crystal Explorer*, (Version 17.5); University of Western Australia, 2012.
(58) Spackman, M. A.; McKinnon, J. J. Fingerprinting Intermolecular Interactions in Molecular Crystals. *CrystEngComm* **2002**, *4* (66), 378−392.
(59) Spackman, M. A.; McKinnon, J. J.; Jayatilaka, D. Electrostatic Potentials Mapped on Hirshfeld Surfaces Provide Direct Insight into Intermolecular Interactions in Crystals. *CrystEngComm* **2008**, *10*, 377−388.
(60) Bondi, A. Van Der Waals Volumes and Radii. *J. Phys. Chem.* **1964**, *68* (3), 441−451.
(61) Batsanov, S. S. Van Der Waals Radii of Elements. *Inorg. Mater.* **2001**, *37* (9), 871−885.
(62) Allen, F. H.; Kennard, O.; Watson, D. G.; Brammer, L.; Orpen, A. G.; Taylor, R. Tables of Bond Lengths Determined by X-Ray and Neutron Diffraction. Part 1. Bond Lengths in Organic Compounds. *J. Chem. Soc., Perkin Trans. 2* **1987**, No. 12, 1−19.
(63) Murugavel, S.; Jacob Prasanna Stephen, C. S.; Subashini, R.; AnanthaKrishnan, D. Synthesis, Structural Elucidation, Antioxidant, CT-DNA Binding and Molecular Docking Studies of Novel Chloroquinoline Derivatives: Promising Antioxidant and Anti-Diabetic Agents. *J. Photochem. Photobiol., B* **2017**, *173*, 216−230.
(64) Wang, C. C.; Chan, C. K.; Lai, C. Y. Environmentally Friendly Nafion-Mediated Friedländer Quinoline Synthesis under Microwave Irradiation: Application to One-Pot Synthesis of Substituted Quinolinyl Chalcones. *Synthesis (Stuttg).* **2020**, *52* (12), 1779−1794.
(65) Bernstein, J.; Davis, R. E.; Shimoni, L.; Chang, N.-L. Patterns in Hydrogen Bonding: Functionality and Graph Set Analysis in Crystals. *Angew. Chem., Int. Ed. Engl.* **1995**, *34* (15), 1555−1573.
(66) Saral, A.; Sudha, P.; Muthu, S.; Irfan, A. Computational, Spectroscopic and Molecular Docking Investigation on a Bioactive Anti-Cancer Drug: 2-Methyl-8-Nitro Quinoline. *J. Mol. Struct.* **2022**, *1247*, 131414.
(67) Uzun, S.; Esen, Z.; Koç, E.; Usta, N. C.; Ceylan, M. Experimental and Density Functional Theory (MEP, FMO, NLO, Fukui Functions) and Antibacterial Activity Studies on 2-Amino-4-(4-Nitrophenyl) −5,6-Dihydrobenzo [h] Quinoline-3-Carbonitrile. *J. Mol. Struct.* **2019**, *1178*, 450−457.
(68) Sayin, K.; Karakaş, D.; Kariper, S. E.; Sayin, T. A. Computational Study of Some Fluoroquinolones: Structural, Spectral and Docking Investigations. *J. Mol. Struct.* **2018**, *1156*, 172−181.
(69) Kesharwani, M. K.; Brauer, B.; Martin, J. M. L. Frequency and Zero-Point Vibrational Energy Scale Factors for Double-Hybrid Density Functionals (and Other Selected Methods): Can Anharmonic Force Fields Be Avoided? *J. Phys. Chem. A* **2015**, *119* (9), 1701−1714.
(70) Garmire, E.; Durfee, C. G.; Storz, T.; Garlick, J.; Hill, S.; Squier, J. A.; Kirchner, M.; Taft, G.; Shea, K.; Kapteyn, H.; Murnane, M.; Backus, S.; Wang, Q.; Liu, Z.; Chen, X.; Fan, S.; Zhang, X.; Zhang, H.; Tao, X.; Li, S.; Rong, H.; Jones, R.; Liu, A.; Cohen, O.; Hak, D.; Fang, A.; Paniccia, M.; Trebino, R.; DeLong, K. W.; Fittinghoff, D. N.; Sweetser, J. N.; Krumbugel, M. A.; Richman, B. A.; Kane, D. J.; Hollemeyer, K.; Altmeyer, W.; Heinzle, E.; Pitra, C.; Wang, G.; König, K.; Halbhuber, K.; Blanche, A.; Bablumian, A.; Voorakaranam, R.; Christenson, C.; Lin, W.; Gu, T.; Flores, D.; Wang, P.; Hsieh, W.; Kathaperumal, M.; Rachwal, B.; Siddiqui, O.; Thomas, J.; Norwood, R. A.; Yamamoto, M. Nonlinear Optics in Daily Life. *Opt. Express* **2013**, *21* (25), 30532−30544.
(71) Satheeshkumar, R.; Montecinos, R.; Vera, A.; Prasad, K. J. R.; Kaminsky, W.; Salas, C. O. Experimental and Theoretical Physicochemical Study of a New Dispirocompound: 4′-(4-Fluorophenyl)-2′,7-Dimethyl-1,4-Dihydro-3H-Dispiro[Cyclopent[b]-Indol-2,5′-[1,2]Oxazinan-6′,3′-Indolin]-2′,3-dione. *J. Mol. Struct.* **2021**, *1227*, 129431.
(72) Kerru, N.; Gummidi, L.; Bhaskaruni, S. V. H. S.; Narayana Maddila, S.; Singh, P.; Jonnalagadda, S. B. A Comparison between Observed and Dft Calculations on Structure of 5-(4-Chlorophenyl)-2-Amino-1,3,4-Thiadiazole. *Sci. Rep.* **2019**, *9*, 19280.

https://doi.org/10.1021/acsomega.3c04360
ACS Omega 2023, 8, 43573−43585